Transient Deformation of Freely-Suspended Liquid Droplets in Electrostatic Fields

R. J. Haywood, M. Renksizbulut, and G. D. Raithby
Mechanical Engineering Dept., University of Waterloo, Waterloo, Ontario, Canada N2L-3G1

The problem of freely-suspended liquid droplets deforming due to an applied electrostatic field is examined. Developed is a numerical model capable of predicting the complete transient histories of droplets in systems with a wide range of dispersed- and continuous-phase densities, viscosities, relative permittivities, and electric field strengths. For liquid/gas systems, the predictions of the numerical model demonstrated that the critical field strength and critical permittivity ratio during actual transient breakup are not necessarily the same as those predicted by steady-state theories. An approximate analytical model of transient droplet deformation is also developed, which is able to predict the deformation time histories for large Ohnesorge number, small-deformation liquid/liquid systems. The approximate analytical model agreed well with the results of the complete numerical model.

Introduction

A fundamental understanding of the behavior of liquid droplets subjected to electrostatic fields is required to resolve problems that arise in many applications. Examples include paint and agricultural sprays, atmospheric phenomena, and ink jet printers. Chemical engineers are particularly interested in the use of electrostatically-induced oscillations of liquid droplets to enhance mass transfer rates in solvent extraction processes.

Up to the present time, most research efforts have been concerned with prediction of the critical field strength leading to droplet rupture, and the prediction of steady or quasisteady droplet shapes in subcritical electric fields. The early work of Wilson and Taylor (1925) and Macky (1931) established that for conducting soap bubbles and water droplets, the critical field strength is given by:

$$E_c^* = C_1\sqrt{\gamma^*/R_0^*} \tag{1}$$

This expression has been substantiated by a number of researchers including: Taylor (1964) (analytical); Garton and Krasucki (1964) (experimental); Brazier-Smith (1971b) (numerical); Miksis (1981) (analytical); Dodgson and Souzou (1987) (analytical); and Inculet and Kromann (1989) (experimental). The value of C_1 is usually taken to be 1.52×10^5 $V/N^{1/2}$. For perfectly-conducting droplets, the limiting aspect ratio was found to be 1.83. Consideration of dielectric droplets has shown two distinct behaviors dependent on the ratio of dispersed- to continuous-phase permittivities. Systems with large permittivity ratios ($K_1/K_2>20.8$) exhibit behavior similar to conducting droplets; a critical field strength exists, and exceeding this value leads to the ejection of mass from sharp conical tips at the poles of the droplet (referred to as tip streaming or jetting). Systems with permittivity ratios below the critical value $K_1/K_2<20.8$ will not form conical tips, and consequently, there is no corresponding critical field strength; the droplet will theoretically accommodate any strength of electric field by sufficient elongation.

Although restricted to small departures from the spherical shape, the work of O'Konski and Thacher (1953) led to a simple closed-form solution expressing the steady eccentricity of droplets in terms of the electrostatic field strength and relevant thermophysical properties. Their approach was to find the eccentricity at which the function expressing the total energy of the system, the sum of electric field, and free surface energy, was a minimum. An energy minimization approach has been the basis for many other analytic and semi-analytic models such as those of Garton and Krasucki (1964) and Dodgson and Souzou (1987).

Because of the potential practical applications, investigation has been made of the steady shapes of charged droplets levitated in electrostatic fields. Basaran and Scriven (1989) used a finite element approach to predict axisymmetric shapes and

Correspondence concerning this article should be addressed to M. Renksizbulut.

stability for such droplets. Adornato and Brown (1983) predicted a locus of field strengths and droplet charge levels for the existence of static droplets using both numerical finite element and analytical perturbation analyses.

The study of transient deformation and breakup of liquid droplets in electrostatic fields is inherently more difficult than its steady counterpart. Analytical studies have examined only limiting cases of inviscid or highly viscous droplets. Brazier-Smith et al. (1971) numerically modeled the transient deformation and breakup of isolated water droplets charged to the Rayleigh (1882) limit and found the droplet to proceed through a series of approximately prolate spheroidal shapes until an aspect ratio 2.5 is reached, when coning occurs at the droplet poles and liquid is assumed to issue. Their model assumes the droplet liquid to be inviscid and ignores interaction with the continuous phase.

Brazier-Smith (1971a) examined the stability of water drops subjected to a step function electric field. Assuming that the droplets maintain a spheroidal shape and ignoring viscous effects, it was shown that the critical field strength under an impulsively applied electric field is less than the critical value from quasisteady analyses.

Using a boundary integral numerical technique, Sherwood (1988) examined viscous droplet deformation over a wide range of permittivity and conductivity ratios. The results typically show the equilibrium shapes of a deforming droplet as the electric field strength is increased in discrete steps toward the critical level. It is suggested that there are two modes of breakup:

1. Tip streaming when the permittivity of the droplet is much greater than that of the surrounding fluid
2. Division into two blobs connected by a thin thread when the conductivity of the droplet is greater than that of the surrounding fluid.

As the supporting evidence of the second type of breakup, the experimental results of Torza et al. (1971, Figure 9, p. 314) are cited for a case where the permittivity and conductivity ratios are 12.7 and 10^5, respectively. Unfortunately, these experimental data do not clarify whether the large conductivity ratio is entirely responsible for this type of breakup as suggested by Sherwood (1988). It is possible that the breakup behavior was equally influenced by the reduced permittivity ratio. No attempt was made to investigate the effect of disparate viscosities in the dispersed and continuous phases. Furthermore, because the model neglects transient terms in the solution of the momentum equations governing the fluid motion in the dispersed and continuous phases, the results are applicable only to problems wherein the viscous diffusion time is very small compared to the relaxation time to equilibrium: $\rho^* R_0^* \gamma^* / \mu^{*2} \ll 1$.

Assuming inviscid flow, Tsamopoulos et al. (1985) analyzed the transient behavior of charged droplet breakup using a powerful analytical technique combining domain perturbation and multiple time-scale methods. The analytical method was validated by comparing the predicted critical charge with results from a finite element calculation for two-, three-, four- and five-lobed static droplet shapes. A similar analytical technique was used by Feng and Beard (1991) to predict resonance phenomena for droplets exposed to alternating electric fields.

Experimental investigations of transient deformation and breakup have covered a wider range of dispersed- and continuous-phase viscosities and permittivities. In many instances, however, the results of these studies seem conflicting and/or inconclusive. Consider, for example, the effect of the dispersed- to continuous-phase permittivity ratio. Allan and Mason (1962) found water droplets suspended in LB-1715 ($K_1/K_2 = \infty$) to show a "tendency toward pointed ends as observed by Wilson and Taylor (1925)." The transient breakup of a water droplet in castor oil ($K_1/K_2 = 12.7$), as recorded by Torza et al. (1971), showed a simple elongation of the droplet into two lobes connected by a thin thread. When classifying transient breakup behavior, however, Allan and Mason (1962) used a system based on the permittivity ratio such that: 1) for $K_1/K_2 = \infty$, the droplet remains spheroidal as the field strength is increased until at E_c it suddenly separates into two approximately equal parts; 2) for $1 < K_1/K_2 < \infty$, the droplet remains spheroidal with increasing E until suddenly one end of the droplet is pulled out into a thin thread that moves directly toward the electrode; and 3) for $K_1/K_2 < 1$, the droplet flattens into a sheet, folds and twists, and eventually breaks up unevenly. Experimental evidence aside, this classification system counters the intuitive expectation that the transient deformation behavior will exhibit qualitative similarity with the steady results: some change in behavior at $K_1/K_2 \approx 20.8$.

More recently, Moriya et al. (1986a) developed an analytical model of transient droplet deformation limited to nearly spherical highly-viscous liquid/liquid systems. Their experimental evidence supported the model that predicted the degree of deformation to be exponential in time:

$$D/D_\infty = 1 - \exp(-t^*/\tau^*) \tag{2}$$

where D is the degree of deformation, and τ^* is the system time constant, $(\mu_1^* + \mu_2^*) R_0^* / \gamma^*$. In a companion article, Moriya et al. (1986b) further investigated burst behavior and found two classes of behavior dependent on the dispersed-phase viscosity. Low-viscosity water droplets burst by ejecting small droplets from conical endpoints, while viscous polymer droplets produced long thin threads from their ends. Most recently, Nishiwaki et al. (1988) examined more closely the system time constant and suggest better agreement with experimental data if it is expressed as $\tau^* = (2\mu_1^* + \mu_2^*) R_0^* / \gamma^*$. This heuristic modification of the theoretically-determined time constant suggests that the actual fluid motion during deformation does not follow the assumed flow on which the theoretical model is based. Because it is difficult to gain a detailed knowledge of the fluid motion from experimental studies, the precise nature of the dispersed- and continuous-phase flow fields is unknown presently. A more complete theoretical analysis of the problem would enhance understanding of the fluid mechanics and perhaps lead to an improved expression of the time constant τ^*.

The steady behavior of deforming liquid droplets subjected to electrostatic fields has been thoroughly studied both theoretically and experimentally. A fundamental aspect of these studies has been to define values of critical field strength and critical permittivity ratio under steady conditions. Transient deformation and breakup have been studied only theoretically in the limit of an inviscid dispersed phase without interaction with the continuous phase, in the limit of highly-viscous dispersed and/or continuous phases, and for highly-viscous systems with very small deformations.

In this article, a numerical method is developed and applied

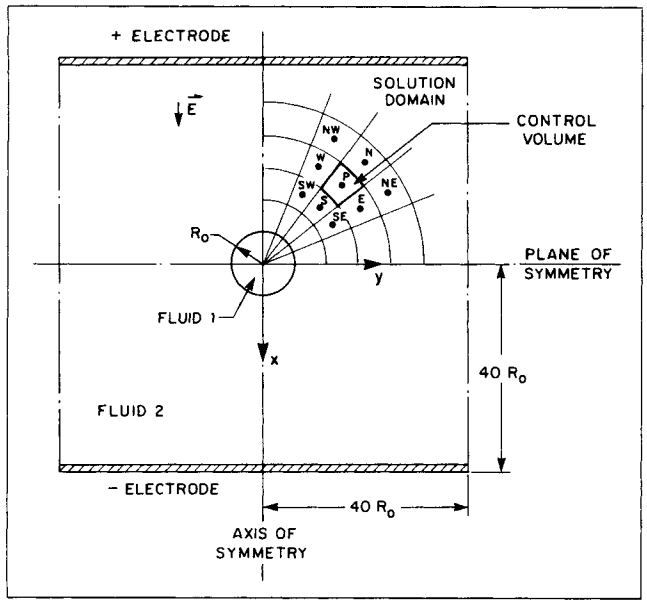

Figure 1. Problem schematic.

to study transient droplet deformation over a wide range of controlling parameters. We attempt to better understand the effects of dispersed to continuous phase ratios of permittivities and viscosities without restriction to small deformations. At present, the values of critical field strength and critical permittivity ratio have been defined for the most part only in steady-state analyses. Since droplet breakup is inherently a transient process, an important objective of the current study is to establish if these values remain unchanged when transient effects are considered. Also presented are the mathematical underpinnings and development of the numerical model require to answer these questions.

The Mathematical Model

Figure 1 shows the problem to be studied. An initially spherical droplet of fluid with density ρ_1^*, viscosity μ_1^*, and relative permittivity K_1 is surrounded by a second fluid (ρ_2^*, μ_2^*, K_2), and is subjected to an electrostatic field arising from the application of DC potentials at electrodes separated a distance of 80 radii. Due to the assumed symmetry, the solution is required over only one quadrant of the problem as indicated in the figure. The following additional assumptions are made: (1) fluid flow is laminar in both phases; (2) there is no effect due to gravity or other external body forces; (3) fluids in both phases are Newtonian with constant physical and electrical properties; (4) ideal electrical properties exist (that is, nonleaky dielectrics, perfect conductors); and (5) the charge relaxation time is much smaller than all other pertinent time scales. Initially, the droplet and its surroundings are assumed to be motionless.

The governing equations nondimensionalized are:

Conservation of mass:

$$\frac{\partial \rho}{\partial t} + \vec{\nabla} \cdot (\rho \vec{v}) = 0 \tag{3}$$

Conservation of momentum:

$$\frac{\partial}{\partial t}(\rho \vec{v}) + \vec{\nabla} \cdot (\rho \vec{v}\,\vec{v}) = -\vec{\nabla} p + Oh_1 \vec{\nabla} \cdot \tilde{\sigma} \tag{4}$$

where

$$\tilde{\sigma} = \mu[\vec{\nabla}\,\vec{v} + (\vec{\nabla}\,\vec{v})^T] \tag{5}$$

Gauss' law:

$$\vec{\nabla} \cdot \vec{\nabla} V = 0 \tag{6}$$

At the droplet surface, the appropriate boundary conditions are:

Continuity of velocity:

$$(\vec{v})_1 = (\vec{v})_2 \tag{7}$$

Continuity of normal stress:

$$[(p\tilde{I} - Oh_1\tilde{\sigma}) \cdot \hat{n}]_1 \cdot \hat{n} = [(p\tilde{I} - Oh_1\tilde{\sigma}) \cdot \hat{n}]_2 \cdot \hat{n} - (2H + 2) - E_0^2[(\vec{\nabla} V \cdot \hat{n})^2(1 - K_2/K_1) + (\vec{\nabla} V \cdot \hat{t})^2(K_1/K_2 - 1)] \tag{8}$$

Continuity of tangential stress:

$$(\tilde{\sigma} \cdot \hat{n}) \cdot \hat{t}\,|_1 = (\tilde{\sigma} \cdot \hat{n}) \cdot \hat{t}\,|_2 \tag{9}$$

Continuity of normal electric potential gradient:

$$K \vec{\nabla} V \cdot \hat{n}\,|_1 = K \vec{\nabla} V \cdot \hat{n}\,|_2 \tag{10}$$

The potential is single valued at the interface:

$$V|_1 = V|_2 \tag{11}$$

The governing equations and boundary conditions are reasonably self-explanatory with the exception of the normal stress condition given by Eq. 8. This equation expresses the pressure discontinuity across the interface as a function of the surface tension force caused by the curved interface and characterized by the mean curvature H, electrostatic forces arising due to unequal permittivities in the two phases and viscous normal stresses arising due to the interface motion. For a more detailed discussion of electrohydrodynamics, see the excellent review by Melcher and Taylor (1969).

The remaining boundary conditions apply at the outer boundary of the solution domain and along the axis and plane of symmetry.

Outer boundary:

$$u = 0 \tag{12}$$

$$v = 0 \tag{13}$$

$$V = x \tag{14}$$

Along the axis of symmetry:

$$\frac{\partial u}{\partial y}=0 \tag{15}$$

$$v=0 \tag{16}$$

$$\frac{\partial V}{\partial y}=0 \tag{17}$$

Along the plane of symmetry:

$$u=0 \tag{18}$$

$$\frac{\partial v}{\partial x}=0 \tag{19}$$

$$V=0 \tag{20}$$

The Numerical Model

A finite volume method using an adaptive grid formed the basis of the numerical technique used to solve the governing equations. This methodology has gained widespread acceptance, and the details of its implementation are well documented in such publications as Patankar (1980) and Minkowycz et al. (1988). Conceptually, the method relies on the formation of linearized algebraic equations through the integration of governing differential equations that express the conservation of some quantity (typically mass, momentum, or energy) over finite control volumes covering the problem domain. For example, consider the convection diffusion equation for the general quantity ϕ. Commencing with the governing equation:

$$\frac{\partial}{\partial t}(\rho\phi)+\vec{\nabla}\cdot(\rho\vec{v}\phi)=\vec{\nabla}\cdot(\Gamma_\phi\vec{\nabla}\phi)+S_\phi \tag{21}$$

Integration is performed over an arbitrary control volume (see Figure 1):

$$\int_{\forall}\frac{\partial}{\partial t}(\rho\phi)d\forall+\int_{\forall}\vec{\nabla}\cdot(\rho\vec{v}\phi)d\forall = \int_{\forall}\vec{\nabla}\cdot(\Gamma_\phi\vec{\nabla}\phi)d\forall+\int_{\forall}S_\phi d\forall \tag{22}$$

For a nonadaptive (i.e., fixed) grid, the transformation of this integral equation into an algebraic equation would be performed at this stage by expressing flux, source and transient terms as approximations written in terms of nodal values. Because the present problem required the control volumes to change size and shape with time, further manipulation of Eq. 22 was necessary. Using Leibnitz's rule, the first integral was expressed over a control volume that needed not be stationary. Using the divergence theorem, the second and third integrals were expressed as surface integrals. The following integral equation is thereby obtained:

$$\frac{d}{dt}\int_{\forall}\rho\phi d\forall+\oint_S\rho\phi(\vec{v}-\vec{v}_S)\cdot\hat{n}dA = \oint_S\Gamma_\phi\vec{\nabla}\phi\cdot\hat{n}dA+\int_{\forall}S_\phi d\forall \tag{23}$$

where $\vec{v}_S$ is the velocity of the control volume surface. Adopting an implicit formulation, the convective and diffusive fluxes, and the source term were approximated over a time step Δt by their values at the new time $t+\Delta t$. Integration and approximation, in terms of nodal values, then resulted in linearized algebraic finite volume equations relating the value of ϕ at P to its eight neighbors as follows (see Figure 1):

$$a_P\phi_P=a_E\phi_E+a_N\phi_N+a_W\phi_W+a_S\phi_S+a_{NE}\phi_{NE}+a_{NW}\phi_{NW}+a_{SW}\phi_{SW}+a_{SE}\phi_{SE}+b_P \tag{24}$$

Temporal derivatives and convective fluxes due to the grid motion, were discretized following the method of Demirdzic and Peric (1988). For a more detailed description of the use of finite volume methods with adaptive grids, see the work by Demirdzic and Peric (1988) and by Demirdzic and Peric (1990).

For easy physical interpretation, primitive variables (Cartesian velocity components u, v, and pressure p) were used in the discrete momentum equations. Rather than using the popular staggered grid approach, the collocated velocity pressure scheme of Peric et al. (1988) was adopted to minimize the cost of grid generation. The SIMPLEC algorithm of Van Doormal and Raithby (1984), in which a truncated form of the momentum equations is substituted into the mass conservation equation, was used in forming an equation for pressure. For those control volumes situated at the droplet surface, the normal stress boundary condition yielded the appropriate pressure equation. Because the SIMPLEC algorithm ensures mass-conserving velocity fields at each iteration, overall conservation of mass was guaranteed for the droplet.

The adaptive curvilinear grid was generated following the method of Thompson et al. (1974). For the current investigation, the numerical grid, although nonorthogonal, was conceptually equivalent to a cylindrical polar system with 30 "tangential" control volumes by 60 "radial" control volumes. Of the 60 radial control volumes, 20 were internal to the droplet. The grid was nonuniform in both phases with the greatest concentration of radial control volumes at the droplet surface. The inner grid and a portion of the outer grid for a moderately deformed droplet are shown in Figure 2. Control volumes of zero thickness were used in the application of boundary conditions at the droplet surface and along the axis and plane of symmetry. The mean curvature H was calculated from the defining relationship $H=-(\vec{\nabla}_s\cdot\hat{n})/2$ based on the discrete local grid geometry.

The numerical solution procedure

The following algorithm was implemented to solve the discrete equations.

Step 1. Values of grid geometry (including droplet shape), velocities, pressures, and electrical potential were available at the beginning of the time step (either from initial conditions or from the previous time step). These values were used as a first estimate of the field variables at the new time $t+\Delta t$.

Step 2. From the current estimate of the velocity fields, the local interface velocities $\vec{v}_s$ prevailing over the time step Δt were calculated.

Step 3. A new numerical grid conforming to the estimated new interface shape at $t+\Delta t$ was calculated.

Step 4. Complete internal and external electrical potential fields were calculated based on the interface shape estimate.

Step 5. The dispersed- and continuous-phase velocity fields were calculated based on the current estimates of the interface velocities $\vec{v}_s$ and dispersed-phase interface pressure of Eq. 8.

Step 6. Dispersed- and continuous-phase pressure corrections were calculated. Dispersed- and continuous-phase velocities (including the interface velocities $\vec{v}_s$) and pressures were corrected via the SIMPLEC algorithm.

Step 7. The relative changes in the just computed and previously iterated values of the velocity, pressure and potential fields were computed. If these changes were less than 10^{-4} and the normal stress and maximum mass residuals were less than 0.1%, convergence was assumed at the new time $t+\Delta t$.

Step 8. Further iteration was performed (i.e., a return to step 2), if convergence criteria were not satisfied. Otherwise, another time step was attempted.

Iterative solvers were used to solve the algebraic equation sets for all the field variables except for the internal droplet pressure field. The internal pressure required a direct solver to maintain stability and to enforce the conservation of mass to the strictest possible tolerances (ensuring that the droplet did not gain or lose mass).

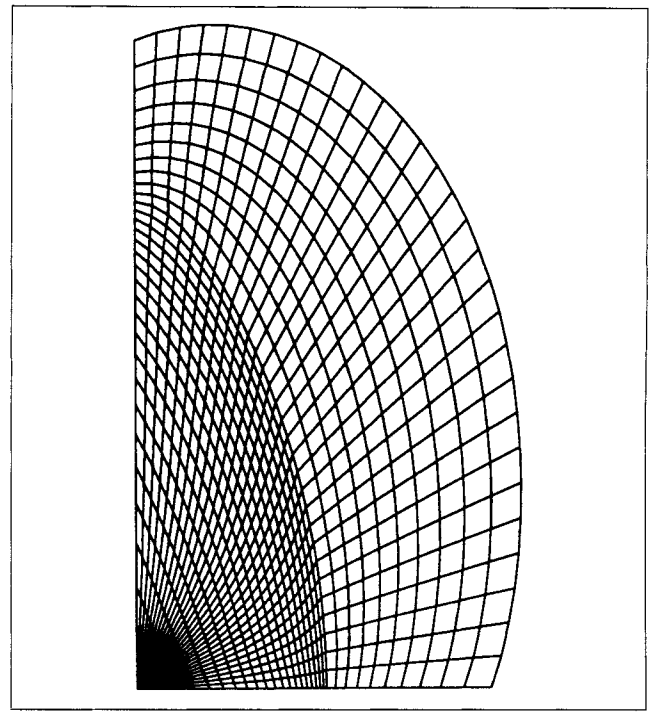

Figure 2. Typical numerical grid.

For clarity, only the first 10 radial control volumes in the continuous phase are shown.

Validation of the numerical model

Because the Fortran code developed for the current numerical model was only a subset of a larger code to be used in predicting convective deformable droplet dynamics, some of the capabilities of the present model were established by comparing them with benchmark solutions for intermediate Reynolds number flows. For laminar flow over solid and liquid spheres ($1<Re<200$), predictions of pressure and friction drag components, wake length, and stagnation pressure were within 1%, and the prediction of the separation point was within 1 degree of the existing experimental and numerical results given in Clift et al. (1978). For laminar flow over oblate and prolate spheroids with aspect ratios up to 0.2, predictions of drag components were within 2%, and the prediction of wake lengths was within 5% of the results given in Clift et al. (1978). These tests fully validated the code for cases in which the surface geometry was fixed.

To validate the numerical model for fluid dynamic problems with interfacial motion, solutions were computed for deforming droplet problems for which analytical solutions and experimental data exist. Data for the limiting case of an inviscid droplet were compared with the results of Brazier-Smith et al. (1971). The numerically-computed aspect ratio history for an initially motionless prolate spheroid of aspect ratio 1.2 was within 2% of the given analytical solution. Numerical predictions of the natural frequency and decay factors of moderately viscous oscillating liquid droplets were compared with experimental (Scott et al., 1990) and numerical (Basaran et al., 1989) results. The numerically-predicted natural frequencies of 0.03- and 0.05-cm water droplets in 2-ethyl-1-hexanol were within 1 and 5% of the experimental values, respectively. Prediction of the decay factor was within 3% of the numerical results of Basaran et al. (1989); but, similar to their result, it was only within 30% of the experimental value. Both the numerical model of Basaran et al. (1989) and the current numerical model ignored the effects of bulk relative motion between the two phases.

When bulk relative motion is present, the increasing oblateness of the droplet must be accompanied by a reduction in the outer-phase dynamic pressure at the equator of the droplet. This reduction in pressure leads to further excitation of the droplet oscillation and results in reduced damping. Hence, the omission of the relative motion appears to be responsible for the poor predictions of the decay factor. It requires a more detailed account to validate the numerical model for viscous dominated systems and to compare to the experimental and theoretical results of Moriya et al. (1986a). This is discussed in the next section.

Grid independence of the numerical results can be assured only for the present problem when the solution has been shown to be insensitive to the following three factors: the level of refinement of the grid in the droplet interior; the level of refinement of the grid in the droplet exterior; and the positioning of the outer boundary where the far field potential and velocity boundary conditions are applied. The solution sensitivity to the proximity of the outer boundary was examined for the problems studied with the largest continuous-phase viscosities. It was found that reducing the outer boundary to within 20 radii from 40 radii typically affected the prediction of aspect ratio by a maximum of 0.1%, the prediction of interface velocities by 0.04%, and the prediction of the interface pressure and surface normal potential gradient by less than 0.01%.

Refinement of the droplet inner grid from 20×20 to 30×30 control volumes resulted in changes in predicted aspect ratio of less than 0.6%, in interface velocities of less than 0.7%, and in the normal potential gradient of less than 0.4%. The solution was the most sensitive to the choice of outer grid refinement and going from 20×20 to 40×30 control volumes resulted in changes in predicted aspect ratio of less than 1.8%, in interface velocities of less than 3.0%, and in the normal potential gradient of less than 2.0%. Further refinement to a 80×40 grid resulted in changes in predicted aspect ratio of less than 0.7%, in interface velocities of less than 0.8%, and in the normal potential gradient of less than 1.0%. The numerical results presented herein (based on a grid of 20×30 interior and 40×30 exterior control volumes with the outer boundary at $40R_0$), are judged to be within 2.0% of the grid-independent solution, reflecting a reasonable compromise between economy and accuracy. Time step independence of the numerical results was verified by the repetition of significant portions of transient solutions with progressively halved time steps (in some cases, transient solutions were repeated in their entirety). Very conservative time steps were utilized throughout the analyses, and in no case did variations amount to greater than 1% in predicting the aspect ratio, velocities, or surface normal potential gradients.

Results and Discussion

In the following study the continuous and dispersed phase densities were restricted to ratios representative of liquid/liquid and liquid/gas systems; $\rho_2/\rho_1=1.0$ and $\rho_2/\rho_1=0.001$, respectively. The results have been presented along these lines. To provide a quick overview of the parametric ranges which were studied, a listing of the pertinent parameters for the numerical simulations is presented in Table 1.

Liquid/liquid systems

By performing a local balance at the droplet surface between viscous, electrostatic, and surface tension normal stresses, Moriya et al. (1986a) developed an analytical model of transient droplet deformation for highly viscous liquid/liquid systems. Assuming small departures from a spherical shape allowed for simple expressions of the electrostatic and surface tension generated stresses to be used in the analysis. Further assuming the rate of viscous diffusion is much faster than the rate of deformation, the velocity fields correspond to steady solutions for simple axisymmetric stagnation flow and analytical expressions are possible for the viscous normal stresses. The resulting model expressing the variation of the deformation parameter D with time is as follows:

$$D=D_\infty[1-\exp(-t^*/\tau^*)] \tag{25}$$

where

$$D_\infty=9K_2\epsilon_0^*R_0^*E_0^{*2}/16\gamma^* \tag{26}$$

$$\tau^*=(\mu_1^*+\mu_2^*)R_0^*/\gamma^* \tag{27}$$

For small deformations ($D_\infty<0.025$), the present numerical results showed excellent agreement with the experimental results of Moriya et al. (1986a). However, their analytical model predicted velocities and pressures that were not generally in good agreement with the results of the complete numerical solution. Close examination showed that Moriya et al. (1986a) failed to enforce the continuity of tangential stress requirement in the solution of the dispersed- and continuous-phase velocity fields. Correcting this deficiency led to the theoretically predicted flow field as shown in Figure 3a which is in excellent agreement with the full numerical solution shown in Figure 3b. The corrected derivation of the velocity fields (detailed in the Appendix) leads to the following analytical result:

$$D=D_\infty[1-\exp(-t^*/\tau^*)] \tag{28}$$

where

$$D_\infty=9K_2\epsilon_0^*R_0^*E_0^{*2}/16\gamma^* \tag{29}$$

$$\tau^*=(\alpha\mu_1^*+\beta\mu_2^*)R_0^*/\gamma^* \tag{30}$$

$$\alpha=\frac{38+47\mu_2^*/\mu_1^*}{40+40\mu_2^*/\mu_1^*} \tag{31}$$

$$\beta=\frac{42+48\mu_2^*/\mu_1^*}{40+40\mu_2^*/\mu_1^*} \tag{32}$$

It is interesting to note that the time constant τ^* of the corrected analytical model in the limiting cases of $\mu_2^*/\mu_1^*\to0$ and $\mu_2^*/\mu_1^*\to\infty$ exhibits behavior in qualitative agreement with the experimental data of Moriya et al. (1986a, Table II, p. 157), *viz.*, $\alpha<1.0$ and $\beta>1.0$, respectively. The corrected analytical model and the results of the full numerical model are shown in Figure 4. It can be seen that the agreement is excellent over the range of $0.001\le\mu_2^*/\mu_1^*\le10.0$.

Because the analytical model is formulated assuming a quasisteady flow field, there was interest in exploring the transient behavior, as the viscous diffusion time was increased. Figure 5 shows the departure of the analytical model from the full numerical model for decreasing dispersed-phase Ohnesorge

Table 1. Summary of Systems Investigated

Liquid/Liquid Systems $\rho_2^*/\rho_1^*=1.0$, $K_1/K_2=1{,}000.0$			
μ_2^*/μ_1^*	$Oh_1=2.00$	$Oh_1=20.0$	$Oh_1=200.0$
0.001	$E_0=0.141$	$E_0=0.141$	$E_0=0.141$
0.100		$E_0=0.387$	$E_0=0.141$
			$E_0=0.316$
1.000		$E_0=0.387$	$E_0=0.141$
10.00	$E_0=0.387$	$E_0=0.316$	$E_0=0.141$
Liquid/Gas Systems $\rho_2^*/\rho_1^*=0.001$, $\mu_2^*/\mu_1^*=0.018$			
K_1/K_2	$Oh_1=1.37\times10^{-3}$	$Oh_1=1.37$	
5.0	$E_0=0.900$		
18.0	$E_0=0.604$		
1,000.0	$E_0=0.297$	$E_0=0.514$	
	$E_0=0.308$		
	$E_0=0.514$		

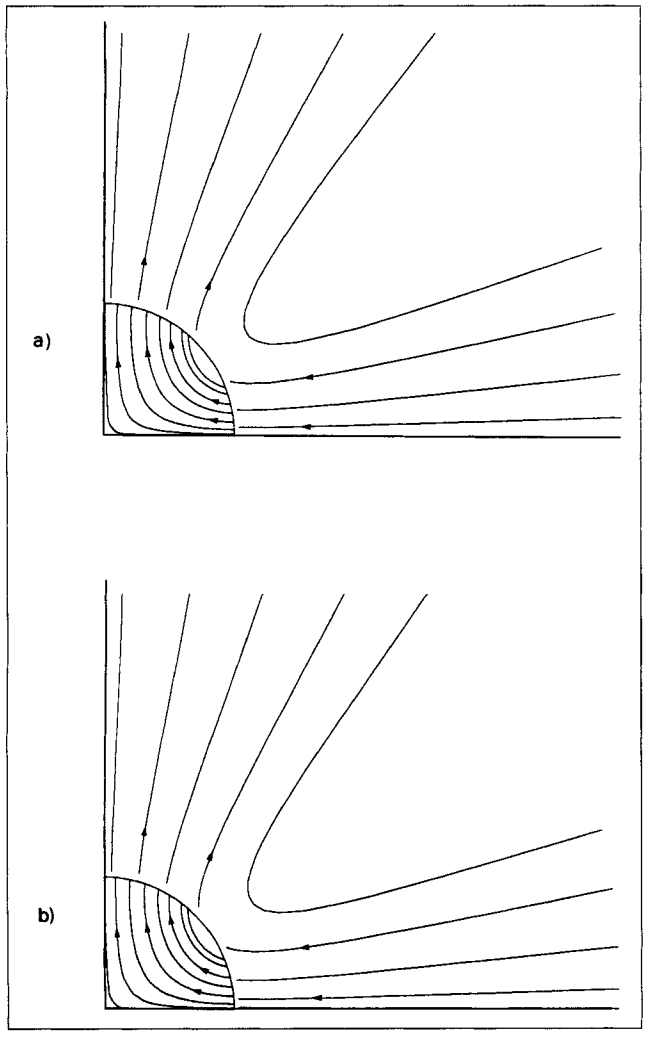

Figure 3. Theoretically-predicted flow fields.

a) Corrected simple model
b) Complete numerical model

The same streamline values have been used in both figures.

number $[Oh = \mu^*/(R_0^* \gamma^* \rho^*)^{1/2}]$. At $Oh_1 = 2$, the error of the analytical model in prediction of the deformation factor at $t^*/\tau^* = 0.10$ and at $t^*/\tau^* = 0.70$ was 53% and 15%, respectively. Clearly, the transient initiation of the fluid motion resulted in the greatest departure from quasisteady behavior at early times. Nevertheless, the approximate analytical model produced reasonable results even at this small Ohnesorge number.

For systems with larger deformations ($D_\infty > 0.025$), the numerical model consistently approached a larger value of D_∞ than predicted by Eq. 29, although the complete numerical solution and approximate analytical model were in agreement at early times. It was felt that an extension of the analytical model to include systems with larger deformations would be both feasible and desirable. By making a detailed examination of the numerical results, the dominant error in the analytical model was found to arise from poor approximations of the variation in the electrical and surface tension stresses with the deformation factor D. For larger deformations, the numerical results showed the electrical stress to be an exponential function of the deformation factor (approximated as constant in the

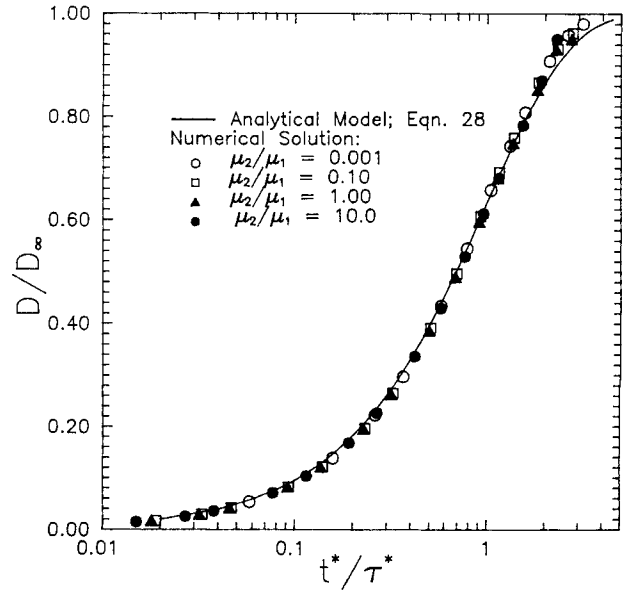

Figure 4. Elongation factor history for viscous liquid/liquid systems.

$E_0 = 0.141$, $D_\infty = 0.024$.

original model) and the normal stress due to surface tension to be quadratic (approximated as linear). Curve fits to the numerically determined variations in these stresses vs. the deformation D yielded the following improved expressions:

$$F_\gamma = -\frac{8\gamma^*}{3R_0^*}(D + 4D^2)(3\cos^2\theta - 1) \tag{33}$$

$$F_E = \frac{9}{2} K_2 \epsilon_0^* E_0^{*2} \exp(5D)\cos^2\theta \tag{34}$$

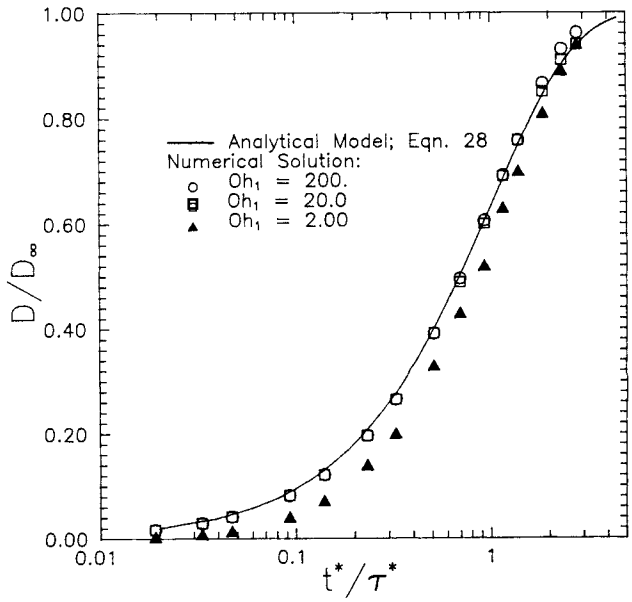

Figure 5. Elongation factor history for liquid/liquid systems: Ohnesorge number effect.

$E_0 = 0.141$, $D_\infty = 0.024$, $\mu_2/\mu_1 = 0.1$.

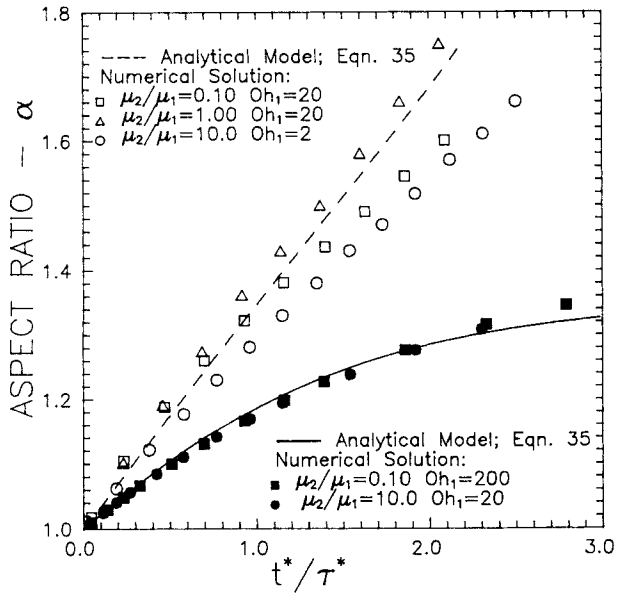

Figure 6. Aspect ratio history for viscous liquid/liquid systems.

Results of the modified analytical and complete numerical models.

These expressions inserted into the stress balance equation yielded the following modified analytical model:

$$\tau^* \frac{dD}{dt^*} = D_\infty \exp(5D) - D - 4D^2 \tag{35}$$

where D_∞, τ^*, α, and β are as defined by Eqs. 29 to 32. The predictive ability of the modified analytical model for systems with large deformations is demonstrated in Figure 6. The prediction of the transient aspect ratio history of the modified analytical model is seen to compare favorably with the results

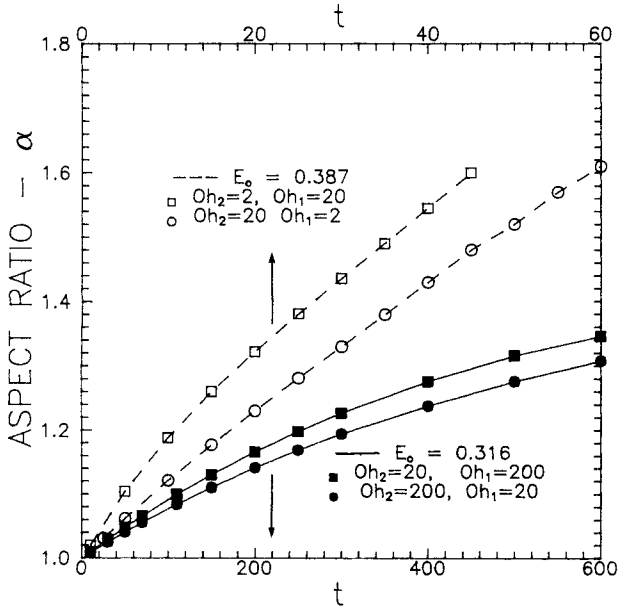

Figure 7. Computed aspect ratio history for viscous liquid/liquid systems: viscosity effect.

of the complete numerical model over a range of viscosities ($0.10 < \mu_2^*/\mu_1^* < 10.0$; $2 < Oh_1 < 200$) and field strengths of $E_0 = 0.316$ and $E_0 = 0.387$.

One final consideration of the liquid/liquid systems was to examine the effects of disparate viscosities in the two phases. From the results of the small deformation analysis, the coefficients α and β indicated that the rate of deformation depends more strongly on the continuous-phase viscosity. The numerical model was used to investigate this dependency for systems with larger deformations, and the results indicated that this trend continues. Figure 7 shows the effect of viscosity ratios of $\mu_2^*/\mu_1^* = 0.10$ and $\mu_2^*/\mu_1^* = 10.0$ on the computed aspect ratio histories of two liquid/liquid systems subjected to moderate electrical fields. Clearly, when the dispersed phase is the controlling phase ($Oh_2/Oh_1 = 0.10$), the deformation proceeds more quickly than when the continuous phase is the controlling phase ($Oh_2/Oh_1 = 10.0$).

Liquid/gas systems

For agricultural and paint sprays and for water droplets in the atmosphere, the continuous- to dispersed-phase density ratios are small. The results in this section are all for $\rho_2/\rho_1 = 0.001$ and should therefore apply to problems in these fields.

Because several of the systems examined in this section proceed to what has been defined as droplet break-up due to tip streaming, it is worth describing the nature of the computations near the point of break-up. At the outset, it should be made clear that the present numerical model requires the control volumes in both phases to remain simply connected so that it is impossible to follow the process of satellite droplet formation. However, it is possible to predict if and when this process will occur with a reasonable degree of certainty. All of the systems studied that underwent break-up exhibited the same qualitative behavior. The elongation proceeded smoothly until the curvature at the droplet tip region changed from convex (Figures 8c and 9c) to concave (Figures 8d and 9d). Following this transition the electrostatically-induced normal stress became so large that the implicit numerical scheme was unable to achieve an interface shape that satisfied the balance of normal stress in the tip region. This was the point at which drop break-up due to tip streaming was assumed to occur. With a sufficiently fine grid it should be possible to track the droplet behavior until the point of incipient break-up and perhaps predict approximately the sizes of satellite droplets. Such a level of grid refinement was not feasible for the current study where interest was in the complete drop history.

Experimental data are available for a water droplet/atmospheric air system in a zero gravity environment (the details of the experiment can be found in Inculet et al., 1990). The measured aspect ratio history for a 14-mm-diameter drop subjected to an electric field of 8 kV/cm is presented in Figure 10. The prediction of the numerical model (the $E_0 = 0.514$ curve) is also shown for comparison. The agreement is within the level of uncertainty in the experimental measurements that results from lack of sharpness in the photographic images. Comparison of the numerically-predicted and experimentally-observed droplet shapes are shown in Figure 8. Despite the generally good agreement, the experimentally observed droplet break-up occurred at a much later time (and at a larger aspect ratio) than the

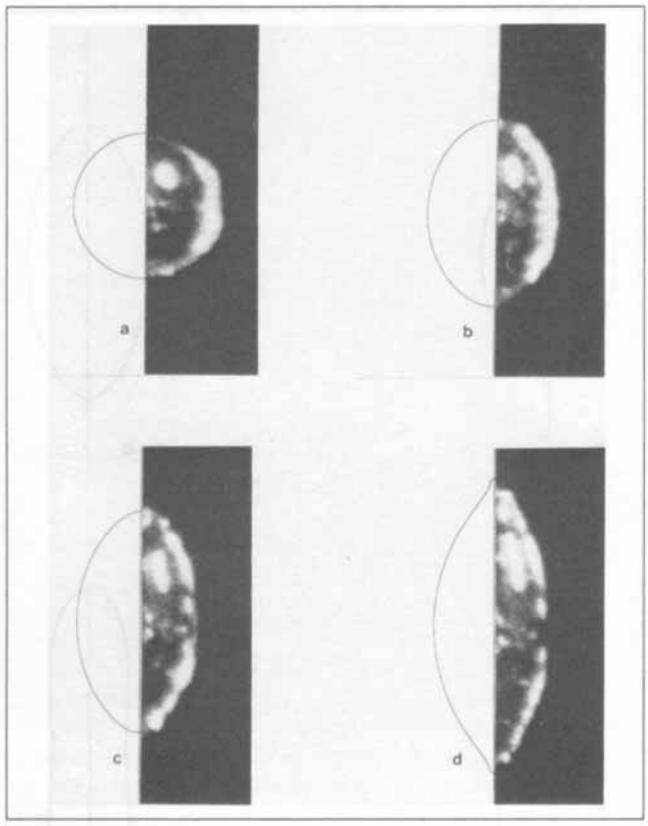

Figure 8. Water droplet in air shape history.

a) $t=0.00$; b) $t=0.25$; c) $t=0.50$; d) $t=0.71$

$E_0=0.514$; $Oh_1=1.37\times10^{-3}$. Experimental results of Inculet et al. (1990).

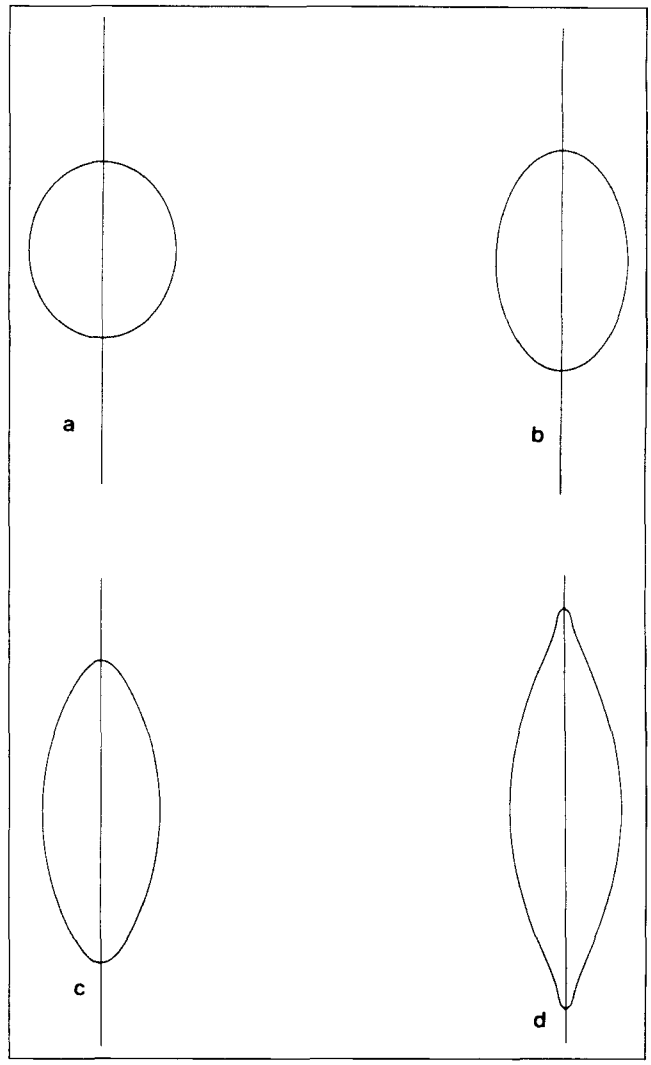

Figure 9. Viscous droplet in air shape history.

a) $t=0.48$; b) $t=1.20$; c) $t=2.16$; d) $t=2.88$.

$E_0=0.514$; $Oh_1=1.37$.

numerical model predicted. The incipient formation of satellite droplets from the poles of the main droplet (tip streaming) was predicted at $t=0.71$ with the aspect ratio = 2.7. We are unable to explain this discrepancy other than to suggest that the experiments may have suffered some decay in the electrical field strength during the droplet life time.

For the previous system, the dispersed-phase Ohnesorge number is 1.3×10^{-3}; viscous effects are negligible. The numerical results showed that the momentum balance was essentially between the pressure gradient (arising due to the large interfacial normal electrical stress) and transient terms (the fluid inertia). In the absence of viscous effects, no mechanism was available to damp the fluid motion. Therefore, it seemed possible that fluid inertial build-up could lead to droplet break-up at a lower critical field strength than that predicted by the steady theory. To test this hypothesis, the numerical model was used to simulate droplet deformation subject to subcritical electric field strengths. It was first established that the numerical model predicted a critical field strength under steady conditions of $E_0=0.325$ (1.6% greater than the accepted value of $E_c=0.320$). The previous (transient) problem was then rerun with field strengths of $E_0=0.297$ and $E_0=0.308$; the aspect ratio histories for these systems are shown in Figure 10. As seen in the figure, the numerical model predicts droplet break-up at a field strength of $E_0=0.308$. This is 3.8% below the accepted critical value developed from steady-state analyses and 5.2% below the numerically-predicted steady value. The numerical results for the $E_0=0.308$ system show the net interfacial stress to be opposing the fluid motion between $t=1.2$ and $t=2.1$. Nevertheless, the fluid inertia is seen to prevail; the droplet elongates sufficiently that the electrical stress again dominates over the restoring surface tension stress, and the droplet proceeds toward break-up.

Comparison with the work of Brazier-Smith (1971a) is very encouraging. Ignoring interaction with the continuous phase, assuming an inviscid flow, and assuming that the droplet maintains a spheroidal shape, Brazier-Smith (1971a) predicted the critical field strength leading to droplet rupture to be between 4 and 6% below the steady value. As pointed out by Brazier-Smith (1971a), this trend is substantiated by experimental evidence; from observations of the break-up of water droplets suddenly exposed to electric fields, Macky (1931) predicted a critical field strength 5.2% below the commonly-accepted steady critical value. In analogy, the analytical results of Tsamopoulos et al. (1985) show charged inviscid droplet break-up occurring at charges below the critical (Rayleigh) limit when

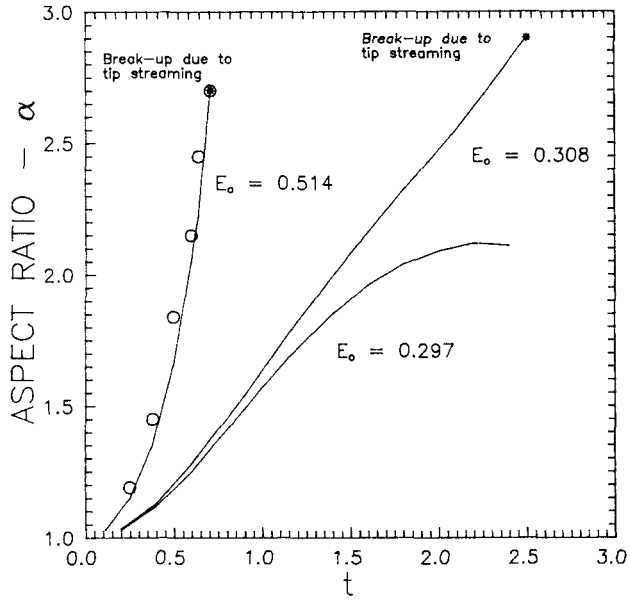

Figure 10. Liquid/gas systems—aspect ratio history.

—, numerical results; o , experimental (Inculet et al., 1990); $Oh_1 = 1.37 \times 10^{-3}$; $\mu_2/\mu_1 = 0.018$.

the droplets are initially subjected to prolate-shape deformations. It is expected that in general the critical field strength for low Ohnesorge number conductive droplets under transient conditions is less than that predicted by steady theory.

In the second liquid/gas system to be modeled numerically, the effects of an increased dispersed-phase Ohnesorge number were investigated. Figures 9 and 11 show the numerically-predicted aspect ratio and shape history respectively for a droplet with $Oh_1 = 1.3$, $E_0 = 0.514$, $K_1/K_2 = 1{,}000$. This would correspond, for example, to a system similar to the previous water/air system but with a thousandfold increase in the dispersed-phase viscosity. As expected, the increased viscosity damps the

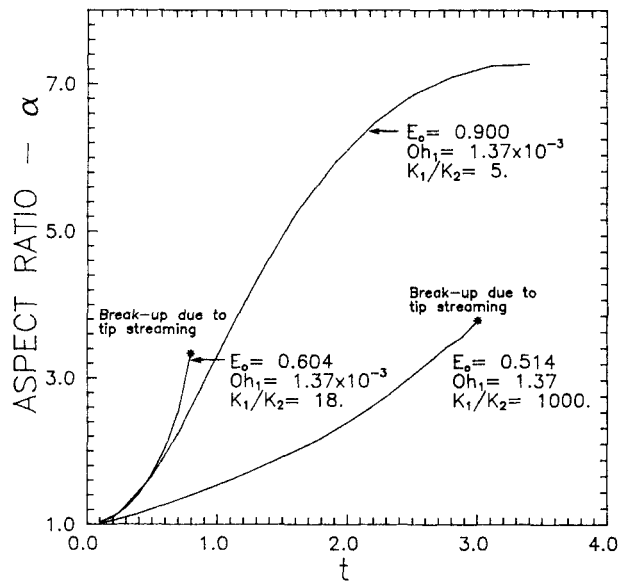

Figure 11. Liquid/gas systems—aspect ratio history: dielectric effect, Ohnesorge number effect.

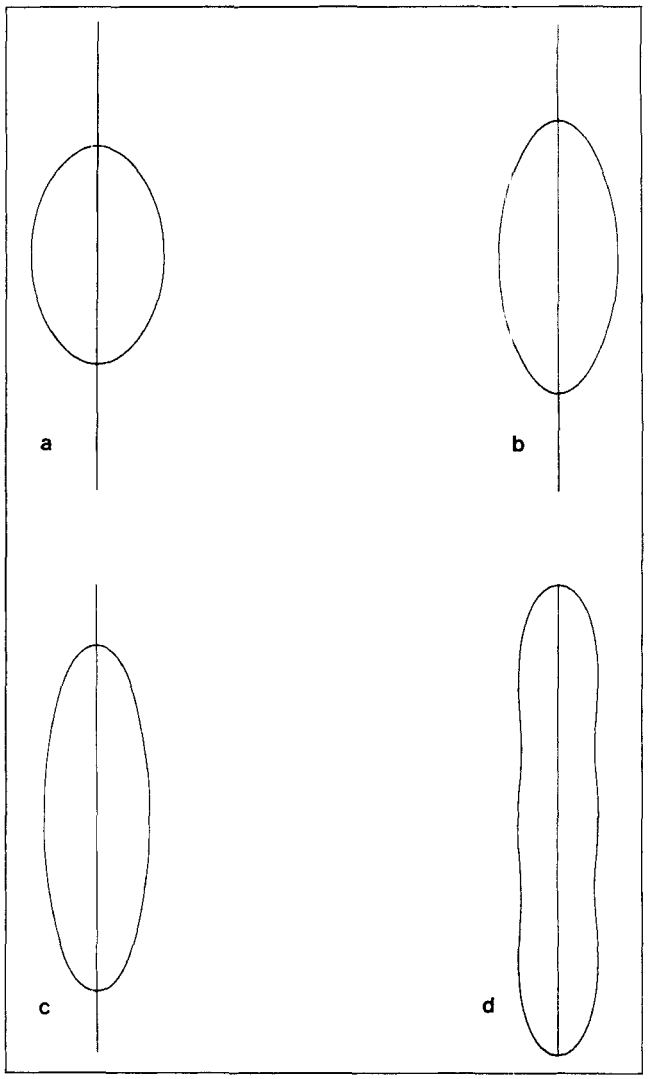

Figure 12. Dielectric droplet in air shape history.

a) $t = 0.50$; b) $t = 0.71$; c) $t = 1.01$; d) $t = 1.91$

$E_0 = 0.900$; $Oh_1 = 1.37 \times 10^{-3}$; $K_1/K_2 = 5$

motion and the droplet deforms more slowly than in the previous system. Also of interest is that the viscosity delays the onset of tip streaming, allowing the droplet to deform to a larger extent (aspect ratio = 3.76) before breakup. Experimental evidence also attests to the ability of highly viscous droplets to produce long ligaments from tip regions without actual breakup. Moriya et al. (1986b) generally found the mode of break-up for systems with large dispersed-phase permittivities ($K_1 \gg K_2$) to depend on the dispersed-phase viscosity. At low viscosities, small droplets were produced from conical endpoints (i.e., tip streaming), while highly viscous polymer droplets produced long, thin threads (see Moriya et al., 1986b, Figure 7, p. 164).

In the final two liquid/gas systems modeled numerically, the behavior of dielectric droplets was examined. From the steady-state theory it is known that for permittivity ratios $K_1/K_2 < 20.8$, no critical field strength exists and the droplet will theoretically accommodate any electric field strength by sufficient elongation. As seen in the previous two cases, above

this critical value ($K_1/K_2 > 20.8$) breakup of the droplet is achieved via tip streaming. Of interest was the behavior of droplets in systems with permittivity ratios near and below this critical ratio. Figures 11 and 12 show the numerical predictions of the transient aspect ratio and shape history for a droplet of $Oh_1 = 1.37 \times 10^{-3}$ with a relative permittivity of 5.0 subjected to an electric field of dimensionless strength $E_0 = 0.900$. The numerical results show zero net interfacial stress at an aspect ratio of approximately 3.0 [in reasonable agreement with the quasisteady model of Sherwood (1988)]; however, the complete transient model predicts that the fluid inertia results in the droplet overshooting this equilibrium position. Later, the net stress on the interface opposes the fluid motion, and the droplet deformation slows and eventually reverses. Computations were not continued beyond the point of maximum deformation. Because the low dispersed- to continuous-phase permittivity ratio inhibits the formation of conical tips at the droplet poles, the "overshoot" phenomenon does not lead to droplet breakup for this system.

When the dispersed- to continuous-phase permittivity ratio is nearer the steady-state critical value, the transient inertial effects are no longer inconsequential. As seen in Figure 11, the numerical model predicts breakup due to tip streaming for a droplet of $Oh_1 = 1.37 \times 10^{-3}$ with a relative permittivity of 18.0 subjected to an electric field of dimensionless strength $E_0 = 0.604$. Physically, the fluid inertia retards fluid motion from equatorial regions of the droplet to the tip regions. Thus, inertial effects inhibit the formation of smooth, rounded poles as seen in the previous problem (Figure 12) and are ultimately responsible for the local drawing of fluid at the polar regions into conical tips (similar to that seen in Figure 8). In this case, breakup due to tip streaming is found to occur at a permittivity ratio 13.5% below the critical value predicted by steady theory.

Conclusions

The numerical model is able to predict the transient histories of deforming liquid droplets subjected to electrostatic fields over a wide range of controlling parameters such as dispersed- and continuous-phase densities, viscosities, relative permittivities, and electric field strengths.

The approximate analytical model of transient droplet deformation is able to predict deformation time histories for large Ohnesorge number, small deformation, liquid/liquid systems, in good agreement with the results of the complete numerical model. Attempts to extend the analytical model to include systems with larger deformations met with reasonable success.

Predictions of the numerical model demonstrated that the critical field strength and critical permittivity ratio during actual transient breakup are not necessarily the same as those predicted by steady-state theories. Numerical results for a low Ohnesorge number conductive liquid droplet in a gaseous environment showed breakup occurring in a "subcritical" electrical field. Although high ($K_1/K_2 = 1{,}000$) and low ($K_1/K_2 = 5.0$) permittivity ratio systems showed behavior that is in qualitative agreement with steady behavior, numerical results showed droplet breakup due to tip streaming occurring at a permittivity ratio of 18.0 (13.5% below the steady-state critical value of 20.8).

Acknowledgment

This work was supported by operating grants and scholarships from the University of Waterloo, the Government of Ontario, and the Natural Sciences and Engineering Research Council. Computations were carried out on a Cray XMP-24 at the Ontario Centre for Large Scale Computation, University of Toronto. The authors would like to thank Professor Ion Inculet for supplying experimental data generously.

Notation

a = coefficient of finite volume equations
A = area
b = source term in finite volume equations
D = deformation factor, $(\alpha - 1)/(\alpha + 1)$
E_0 = dimensionless field strength, $E_0^*(\epsilon_0^* R_0^*/2\gamma^*)^{1/2}$
F = stress acting on interface
H = mean curvature, $-1/2(1/r_1 + 1/r_2)$
$\tilde{I}$ = identity tensor
k = viscosity ratio, μ_2^*/μ_1^*
K = relative permittivity, ϵ^*/ϵ_0^*
m = mass
n_x, n_y = components of unit normal
$\hat{n}$ = unit normal vector
Oh = Ohnesorge number, $\mu^*/(R_0^* \gamma^* \rho^*)^{1/2}$
p = pressure, $p^* R_0^*/\gamma^*$
r_1, r_2 = principle radii of curvature
R = radius of equivalent volume sphere
S = source term
t = time, $t^*(\gamma^*/\rho_1^* R_0^{*3})^{1/2}$
$\hat{t}$ = unit tangent vector
v = velocity component, $\vec{v} = \vec{v}^*(\rho_1^* R_0^*/\gamma^*)^{1/2}$
V = electrostatic potential, $V^*/E_0^* R_0^*$
$\mathcal{V}$ = volume
x = axial distance in cylindrical coordinate system, x^*/R_0^*
y = radial distance in cylindrical coordinate system, y^*/R_0^*
u = velocity component in x coordinate direction
v = velocity component in y coordinate direction

Greek letters

α = aspect ratio (major axis length)/(minor axis length)
α = coefficient defined by Eq. 30
β = coefficient defined by Eq. 31
γ = surface tension
Γ = scalar transport diffusion coefficient
ϵ_0 = permittivity of free space
μ = viscosity, μ^*/μ_1^*
ρ = density, ρ^*/ρ_1^*
$\tilde{\sigma}$ = viscous stress tensor, $\tilde{\sigma} = \tilde{\sigma}^*(\rho_1^* R_0^{*3}/\gamma^*)^{1/2}/\mu_1^*$
τ = time constant
ϕ = generalized variable
Ψ = stream function

Subscripts and superscripts

$\hat{}$ = unit vector
$\vec{}$ = vector
$\tilde{}$ = tensor
* = dimensional quantity
0 = initial value
1 = dispersed phase (droplet)
2 = continuous phase (surroundings)
∞ = at steady state
c = critical
P = at the control volume center
r = radial component
θ = tangential component
s = at the droplet surface
S = at the control volume surface
T = transpose

Literature Cited

Adornato, P. M., and R. A. Brown, "Shape and Stability of Electrostatically Levitated Drops," *Proc. R. Soc. A*, **389**, 101 (1983).

Allan, R. S., and S. G. Mason, "Particle Behavior in Shear and Electric Fields: I. Deformation and Burst of Fluid Drops," *Proc. R. Soc. A*, **267**, 45 (1962).

Basaran, O. A., T. C. Scott, and C. H. Byers, "Drop Oscillations in Liquid-Liquid Systems," *AIChE J.*, **35**(8), 901 (1989).

Basaran, O. A., and L. E. Scriven, "Axisymmetric Shapes and Stability of Charged Drops in an Electric Field," *Phys. Fluids A*, **1**(5), 799 (1989).

Brazier-Smith, P. R., "The Stability of a Water Drop Oscillating with Finite Amplitude in an Electric Field," *J. Fluid Mech.*, **50**(3), 417 (1971a).

Brazier-Smith, P. R., "Stability and Shape of Isolated and Pairs of Water Drops in an Electric Field," *Phys. Fluids*, **14**(1), 1 (1971b).

Brazier-Smith, P. R., S. G. Jennings, and J. Latham, "An Investigation of the Behavior of Drops and Drop-pairs Subjected to Strong Electrical Forces," *Proc. R. Soc. A*, **325**, 363 (1971).

Clift, R., J. R. Grace, and M. E. Weber, *Bubbles, Drops and Particles*, Academic Press, New York (1978).

Demirdzic, I., and M. Peric, "Space Conservation Law in Finite Volume Calculations of Fluid Flow," *Int. J. Num. Methods Fluids*, **8**, 1037 (1988).

Demirdzic, I., and M. Peric, "Finite Volume Method for Prediction of Fluid Flow in Arbitrarily Shaped Domains with Moving Boundaries," *Int. J. Num. Methods Fluids*, **10**, 771 (1990).

Dodgson, N., and C. Sozou, "The Deformation of a Liquid Drop by an Electric Field," *J. Appl. Math. Phys. (ZAMP)*, **38**, 424 (1987).

Feng, J. Q., and K. V. Beard, "Resonances of a Conducting Drop in an Alternating Electric Field," *J. Fluid Mech.*, **222**, 417 (1991).

Garton, C. G., and Z. Krasucki, "Bubbles in Insulating Liquids: Stability in an Electric Field," *Proc. R. Soc. A*, **280**, 211 (1964).

Inculet, I. I., J. M. Floryan, and R. J. Haywood, "Dynamics of Water Droplet Break-Up in Electric Fields," IEEE IAS Meeting, Seattle (1990).

Inculet, I. I., and R. Kromann, "Break-Up of Large Water Droplets by Electric Fields," *IEEE Trans. Ind. Appl.*, **25**(5), 945 (1989).

Langlois, W. E., *Slow Viscous Flow*, Macmillan, New York (1964).

Macky, W. A., "Some Investigations of the Deformation and Breaking of Water Drops in Strong Electric Fields," *Proc. R. Soc. A*, **133**, 565 (1931).

Melcher, J. R., and G. I. Taylor, "Electrohydrodynamics: A Review of the Role of Interfacial Shear Stresses," *Ann. Rev. Fluid Mech.*, **1**, 111 (1969).

Miksis, M. J., "Shape of a Drop in an Electric Field," *Phys. Fluids*, **24**(11), 1967 (1981).

Minkowycz, W. J., E. M. Sparrow, G. E. Schneider, and R. H. Pletcher, *Handbook of Numerical Heat Transfer*, Wiley, New York (1988).

Moriya, S., K. Adachi, and T. Kotaka, "Deformation of Droplets Suspended in Viscous Media in an Electric Field: 1. Rate of Deformation," *Langmuir*, **2**, 155 (1986a).

Moriya, S., K. Adachi, and T. Kotaka, "Deformation of Droplets Suspended in Viscous Media in an Electric Field: 2. Burst Behavior," *Langmuir*, **2**, 161 (1986b).

Nishiwaki, T., K. Adachi, and T. Kotaka, "Deformation of Viscous Droplets in an Electric Field: Poly(propylene)/Poly(dimethylsiloxane) Systems," *Langmuir*, **4**, 170 (1988).

O'Konski, C. T., and H. C. Thacher, "The Distortion of Aerosol Droplets by an Electric Field," *J. Phys. Chem.*, **57**, 955 (1953).

Patankar, S. V., *Numerical Heat Transfer and Fluid Flow*, McGraw-Hill, New York (1980).

Peric, M., R. Kessler, and G. Scheurer, "Comparison of Finite-Volume Numerical Methods with Staggered and Collocated Grids," *Computers and Fluids*, **16**(4), 389 (1988).

Rayleigh, J. W. S., "On the Equilibrium of Liquid Conducting Masses Charged with Electricity," *Phil. Mag.*, **14**, 184 (1882).

Scott, T. C., O. A. Basaran, and C. H. Byers, "Characteristics of Electric Field Induced Oscillations of Translating Liquid Droplets," *Ind. Eng. Chem. Res.*, **29**(5), 901 (1990).

Sherwood, J. D., "Break-Up of Fluid Droplets in Electric and Magnetic Fields," *J. Fluid Mech.*, **188**, 133 (1988).

Taylor, G. I., "Disintegration of Water Drops in an Electric Field," *Proc. R. Soc. A*, **280**, 383 (1964).

Thompson, J. F., F. C. Thames, and C. W. Mastin, "Automatic Numerical Generation of Body-Fitted Curvilinear Coordinate System for Field Containing Any Number of Arbitrary Two-Dimensional Bodies," *J. Comp. Phys.*, **15**, 299 (1974).

Torza, S., R. G. Cox, and S. G. Mason, "Electrohydrodynamic Deformation and Burst of Liquid Drops," *Phil. Trans. R. Soc. Lond. A*, **269**, 295 (1971).

Tsamopoulos, J. A., T. R. Akylas, and R. A. Brown, "Dynamics of Charged Droplet Break-Up," *Proc. R. Soc. A*, **401**, 67 (1985).

Van Doormaal, J. P., and G. D. Raithby, "Enhancements of the Simple Method for Predicting Incompressible Fluid Flow," *Num. Heat Transfer*, **7**, 147 (1984).

Wilson, C. T. R., and G. I. Taylor, "The Bursting of Soap Bubbles in a Uniform Electric Field," *Proc. Cambridge Phil. Soc.*, **22**, 728 (1925).

Appendix: Simple Analytical Model of Transient Droplet Deformation

To make this Appendix more readable, dimensional quantities have not been demarcated by a superscript asterisk as in the rest of the article. Following Moriya (1986a), the interfacial normal stress balance is expressed:

$$p_2 - \sigma_{2,rr} = p_1 - \sigma_{1,rr} + F_\gamma + F_E \tag{A1}$$

For small deformations ($D < 0.025$), the surface tension and electrical normal stresses are approximately:

$$F_\gamma = -\frac{8D_\gamma}{3R_0}(3\cos^2\theta - 1) \tag{A2}$$

$$F_E = \frac{9\epsilon_0 K_2}{2} E_0^2 \cos^2\theta \tag{A3}$$

To complete the simple model, an expression giving the normal stress due to the fluid motion $p - \sigma_{rr}$ in terms of the deformation rate is required. Assuming that the viscous diffusion rate is much faster than the deformation rate, the transient and inertial terms can be neglected and the equation of motion becomes:

$$\vec{\nabla} p = \vec{\nabla} \cdot \tilde{\sigma} \tag{A4}$$

The solution is given in the form of Stokes stream function:

$$\Psi = \left(C_1 \frac{R_0^4}{r^2} + C_2 R_0^2 + C_3 \frac{r^3}{R_0} + C_3 \frac{r^5}{R_0^3}\right) \sin^2\theta\cos\theta \tag{A5}$$

$$u_r = \frac{1}{r^2 \sin\theta} \frac{\partial \Psi}{\partial \theta} \tag{A6}$$

$$u_\theta = \frac{1}{r\sin\theta} \frac{\partial \Psi}{\partial r} \tag{A7}$$

The boundary conditions, at the interface, origin, and far from the droplet are as follows:

$$\vec{u}_1 = \textbf{finite} \quad \mathbf{r} = \mathbf{0} \tag{A8}$$

$$\vec{u}_2 = \textbf{finite} \quad \mathbf{r} = \infty \tag{A9}$$

$$u_{1,r} = u_{2,r} \quad r = R_0 \tag{A10}$$

$$u_{1,\theta} = u_{2,\theta} \quad r = R_0 \tag{A11}$$

$$\sigma_{1,r\theta} = \sigma_{2,r\theta} \quad r = R_0 \tag{A12}$$

Solution of Eqs. A6 and A7 subject to the conditions A8 through A12 leads to the following expressions for the velocities and pressures (in agreement with the analytical results of Torza et al., 1971, Eqs. 42a-42d, p. 304)].

$$u_{1,r} = \left(C_3 \frac{r}{R_0} + C_4 \frac{r^3}{R_0^3} \right) (3\cos^2\theta - 1) \tag{A13}$$

$$u_{1,\theta} = \left(-3C_3 \frac{r}{R_0} - 5C_4 \frac{r^3}{R_0^3} \right) \sin\theta\cos\theta \tag{A14}$$

$$p_1 = p_0 + 7\mu_1 C_4 \frac{r^2}{R_0^3} (3\cos^2\theta - 1) \tag{A15}$$

$$u_{2,r} = \left(C_1 \frac{R_0^2}{r^2} + C_2 \frac{R_0^4}{r^4} \right) (3\cos^2\theta - 1) \tag{A16}$$

$$u_{2,\theta} = 2C_2 \frac{R_0^4}{r^4} \sin\theta\cos\theta \tag{A17}$$

$$p_2 = p_\infty + 2\mu_2 C_1 \frac{R_0^2}{r^3} (3\cos^2\theta - 1) \tag{A18}$$

where

$$C_1 = \frac{2R_0}{3} \frac{dD}{dt} \left(\frac{19/2 + 16k/2}{5 + 5k} \right) \tag{A19}$$

$$C_2 = -\frac{2R_0}{3} \frac{dD}{dt} \left(\frac{9/2 + 6k/2}{5 + 5k} \right) \tag{A20}$$

$$C_3 = \frac{2R_0}{3} \frac{dD}{dt} \left(\frac{8 + 19k/2}{5 + 5k} \right) \tag{A21}$$

$$C_4 = -\frac{2R_0}{3} \frac{dD}{dt} \left(\frac{3 + 9k/2}{5 + 5k} \right) \tag{A22}$$

and:

$$k = \mu_2/\mu_1 \tag{A23}$$

The physical component of the complete normal viscous stress is given by Langlois (1964) as:

$$\sigma_{rr} = 2\mu \frac{\partial v_r}{\partial r} \tag{A24}$$

yielding

$$p_1 - \sigma_{1,rr} = p_0 - \frac{2\mu_1}{3} \frac{dD}{dt} \left(\frac{19 + 47k/2}{5 + 5k} \right) (3\cos^2\theta - 1) \tag{A25}$$

$$p_2 - \sigma_{2,rr} = p_\infty + \frac{2\mu_2}{3} \frac{dD}{dt} \left(\frac{21 + 24k}{5 + 5k} \right) (3\cos^2\theta - 1) \tag{A26}$$

Substitution of Eqs. A25, A26, A2 and A3 into the normal stress balance (Eq. A1) leads to the simple model as given by Eqs. 28 through 32.

Manuscript received Feb. 18, 1991, and revision received July 17, 1991.